LETTERS
PUBLISHED ONLINE: 2 NOVEMBER 2014 | DOI: 10.1038/NGEO2279
nature geoscience

Earthquake size distribution in subduction zones linked to slab buoyancy

Tomoaki Nishikawa* and Satoshi Ide

The occurrence of subduction zone earthquakes is primarily controlled by the state of stress on the interface between the subducting and overriding plates. This stress state is influenced by tectonic properties, such as the age of the subducting plate and the rate of plate motion[1–4]. It is difficult to directly measure stress on a plate interface. However, the stress state can be inferred using the Gutenberg–Richter relationship's[5] *b*-value, which characterizes the relative number of small compared to large earthquakes and correlates negatively with differential stress[6–13]. That is, a subduction zone characterized by relatively frequent large earthquakes has a low *b*-value and a high stress state. The *b*-value for subduction zones worldwide varies significantly[14,15], but the source of this variance is unclear. Here we use the Advanced National Seismic System earthquake catalogue to estimate *b*-values for 88 sections in different subduction zones globally and compare the *b*-values with the age of the subducting plate and plate motions. The *b*-value correlates positively with subducting plate age, so that large earthquakes occur more frequently in subduction zones with younger slabs, but there is no correlation between *b*-value and plate motion. Given that younger slabs are warmer and more buoyant, we suggest that slab buoyancy is the primary control on the stress state and earthquake size distribution in subduction zones.

It is important to identify the factors that control earthquake occurrence. Pioneering studies over the past three decades[2,3,16] have suggested that the plate convergence rate and age of the subducting plate determine the maximum earthquake size in subduction zones. A young, light plate subducting at a high rate produces a compressive stress field and great earthquakes (Chilean-type), whereas an old heavy slab subducting slowly yields an extensional stress field with low seismicity (Marianas-type). However, this model is inconsistent with the 2004 Sumatra and 2011 Tohoku–Oki earthquakes, and recent studies have proposed different interpretations. For example, trench sediment thickness and tectonic stresses applied on the plate interface may control the maximum earthquake size[17], and the seismicity of medium to large earthquakes is directly controlled by the convergence rate in Marianas-type subduction zones[18].

The stress state is obviously an important control on earthquake occurrence. Although the direct measurement of stress state is difficult, a relationship between stress state and some parameters from earthquake statistics have been proposed. Among several candidates, a parameter that is strongly related to shear stress is the *b*-value, which is the slope of a power-law frequency–size distribution of earthquakes[5]. A negative correlation between *b*-values and ambient shear stress levels has been suggested from laboratory experiments[6–8], and by comparison with earthquake depths[9], focal mechanisms[10] and slip patterns[11,12]. Decreases in *b*-values before great earthquakes can be explained by temporal increases in stress levels during the build-up to the seismic event[13].

The *b*-value shows statistically significant differences among Earth's subduction zones[14,15]. For example, *b*-values in the Tonga–Kermadec and Marianas subduction zones are higher than those in the eastern Pacific subduction zones. Given the relationship between the *b*-value and stress state in the crust, it is anticipated that differences in *b*-values among global subduction zones are due to variations in the stress state in subduction zones. Here we test this hypothesis by comparing the *b*-value with plate age, plate convergence rate, and trench normal component of upper plate velocity with respect to the mantle (Fig. 1a and Supplementary Fig. 1), which are thought to control the stress state in subduction zones via slab buoyancy[1], the preferred trajectory of the slab[2,3], and the resistive sea anchor force acting on the slab[4].

We divided Earth's subduction zones into 145 half-overlapping study regions (Fig. 1a) following ref. 18. Each region is bordered by a trench section of about 500 km defined by the plate model PB2002 (ref. 19) and extends for 200 km in the direction of relative plate motion (Fig. 1b). In each region, earthquakes occurring from 1978 to 2009 in all depth ranges were extracted from the Advanced National Seismic System (ANSS) catalogue. Not only earthquakes on the plate interface, but also those in the overriding plate and intra-slab earthquakes were included. Then we calculated the completeness magnitude M_c for each region following ref. 20. *b*-values were calculated using the maximum-likelihood method[21] (Fig. 1c). At least 100 events were required to calculate accurate *b*-values in each region, and we did not estimate *b*-values for regions where M_c cannot be estimated precisely (see Methods). Consequently, we were unable to estimate *b*-values for the Alaska, Cascadia, Lesser Antilles and southern Chile subduction zones, among others. Ultimately, we were able to estimate *b*-values for 88 of the 145 study regions.

Figure 2 and Supplementary Table 1 show the estimated *b*-values for the 88 regions. The estimated *b*-values, which range from 0.7 to 1.5, are generally low in eastern Pacific subduction zones (Mexico, Costa Rica, Columbia and Chile) and are highly variable in subduction zones of the western Pacific. The Izu–Marianas, Kermadec, Philippines and Java subduction zones have high *b*-values ($\geq$1.3), whereas the Sumatra, Nankai, Puysegur, Solomon Islands and New Hebrides subduction zones have low *b*-values (about 0.9).

We then compared the estimated *b*-values with plate age[22], plate convergence rate[19], and trench normal upper plate velocity in the direction away from the trench[23]. They are defined by the mean value at each trench section. A positive correlation exists between the *b*-value and plate age ($R = 0.60$) (Fig. 3a), whereas the convergence rate and the trench normal upper plate velocity are not well correlated with the *b*-value ($R = 0.22$ and $R = -0.02$)

Department of Earth and Planetary Science, University of Tokyo, Hongo 7-3-1, Bunkyo, Tokyo 113-0033, Japan. *e-mail: nishikawa@eps.s.u-tokyo.ac.jp

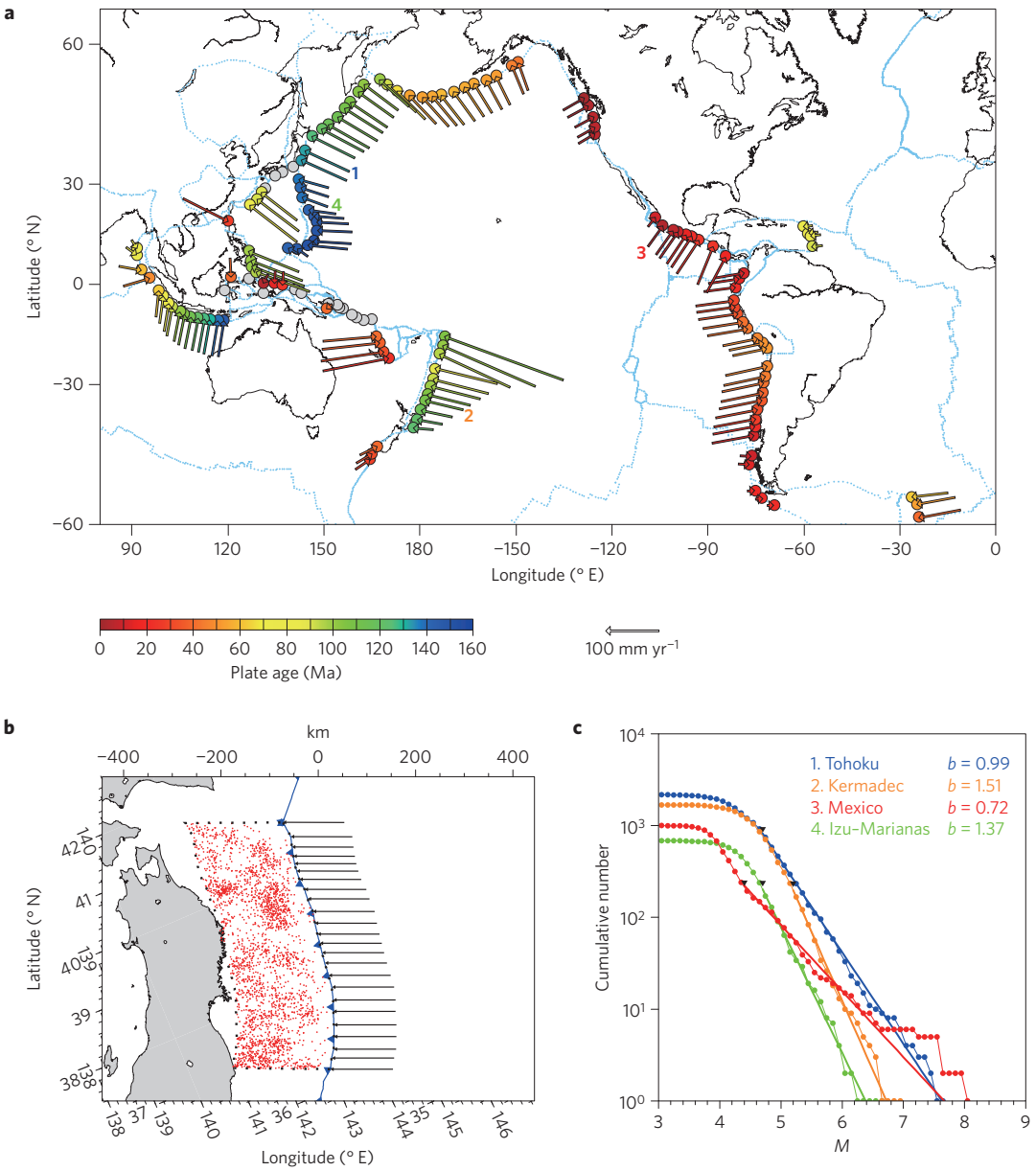

Figure 1 | Summary of *b*-value estimation. a, Locations of the 145 study regions with plate age and convergence rate. The colour of each circle and length of each arrow indicate the plate age and convergence rate, respectively. The grey circles indicate regions where the plate age is poorly constrained. **b**, Study region in Tohoku with hypocentres (red circles) and relative plate motion. Blue line and tooth marks represent trench. **c**, Frequency–magnitude distribution for events in four different regions. Their locations are indicated 1–4 in **a**. The *b*-values represent the slope and the black inverted triangles indicate M_c.

(Fig. 3b,c). Subduction zones with young slabs, such as Mexico, New Hebrides and Chile, are associated with lower *b*-values. In contrast, subduction zones with old slabs such as Kermadec and Marianas have higher *b*-values. This correlation is consistent with a simple model where the slab buoyancy, which depends on the age of the subducting plate, determines the stress state and the *b*-value or the slope of earthquake size distribution in each subduction zone (Fig. 4). A young and buoyant slab produces high normal stress on the plate interface and increases the shear stress, thereby enabling seismic slip, whereas an old and heavy slab reduces both normal and shear stresses on the plate interface. The convergence rate and the upper plate velocity are only weakly correlated with the *b*-value. Furthermore, the observed weak correlations are against the expectation from the mechanical models of subduction zones[2–4]. Because larger convergence rates and larger trenchward upper plate velocities are thought to be associated with higher shear stress in the models, we expect a negative correlation between convergence rate and *b*-value and a positive correlation between trench normal upper plate velocity (measured in the direction away from the trench) and *b*-value. However, both Fig. 3b and c show weak, but opposite correlations. These results suggest that the horizontal force balance, which the convergence rate or the upper plate velocity have been thought to mainly control, may have less influence on the stress state in subduction zones than the vertical balance, which is dominated by the slab buoyancy force.

A more detailed examination of Fig. 3a shows that the goodness of the correlation changes between 60 Ma and 90 Ma. For example, *b*-values for regions with slabs younger than 80 Ma (apart from Sumatra) show a positive correlation with plate age ($R = 0.51$), which contrasts with much weaker correlation ($R = 0.01$) for regions with slabs older than 80 Ma. This change in the goodness of the correlation may correspond to a change in the growth rate of oceanic

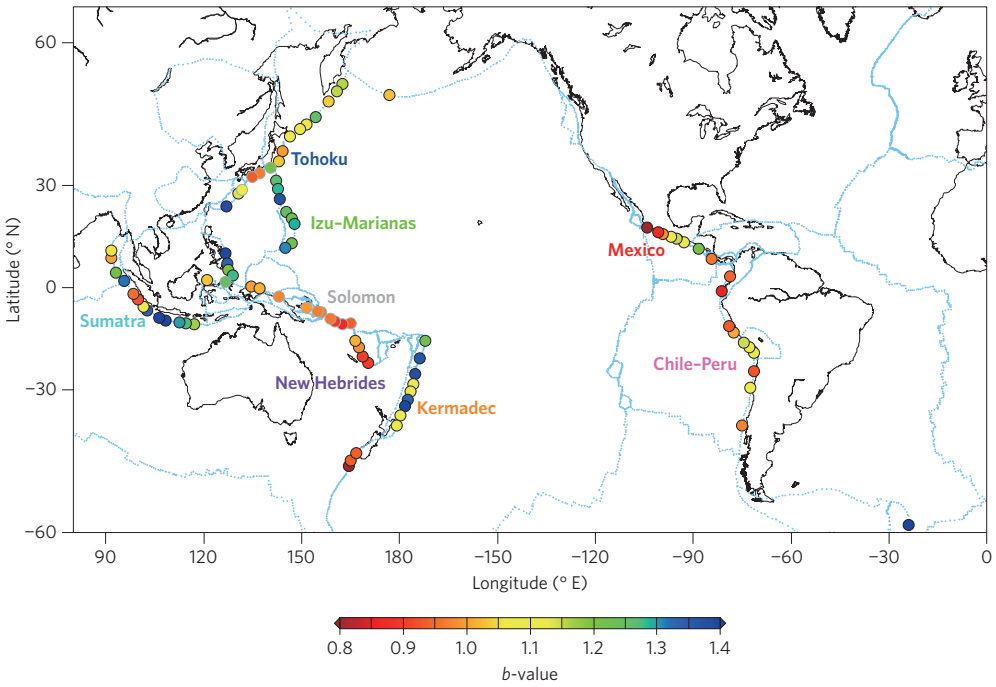

Figure 2 | The 88 study regions with estimated *b*-values. The colour of each circle indicates the *b*-value. Circles with grey outlines indicate regions where the plate age is poorly constrained. In the subsequent correlation analysis, we used *b*-values for 75 regions where the plate age is well constrained.

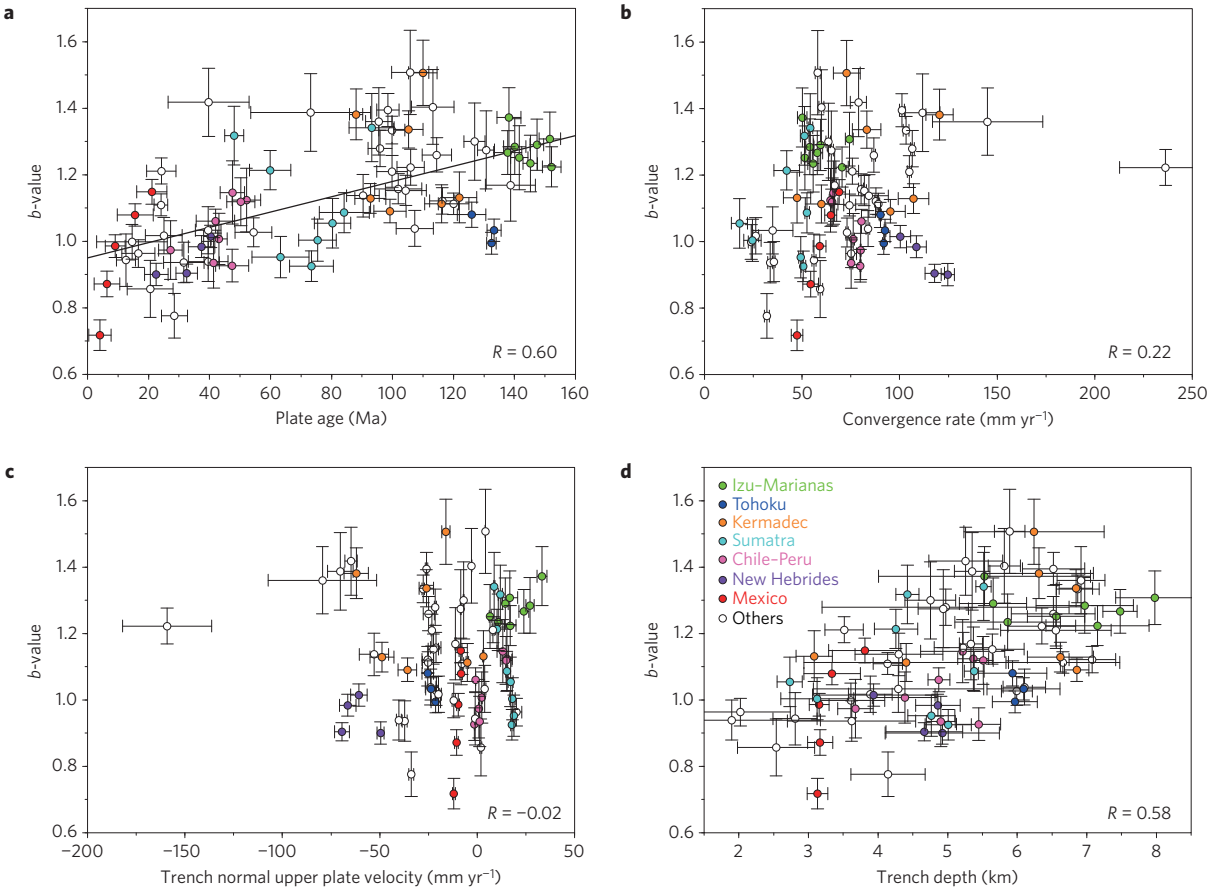

Figure 3 | Comparison between tectonic properties and estimated *b*-values. a, Relationship between plate age and *b*-value. The solid line shows the regression line. **b**, Relationship between convergence rate and *b*-value. **c**, Relationship between trench normal upper plate velocity and *b*-value. Trench normal upper plate velocity is taken negative in the trenchward direction. **d**, Relationship between trench depth and *b*-value. The colours of circles indicate different subduction zones (the key in **d** applies to all panels). The uncertainty estimates for *b*-values are according to ref. 21. The uncertainty estimates for tectonic properties are estimated from the underlying model errors and along-strike variations.

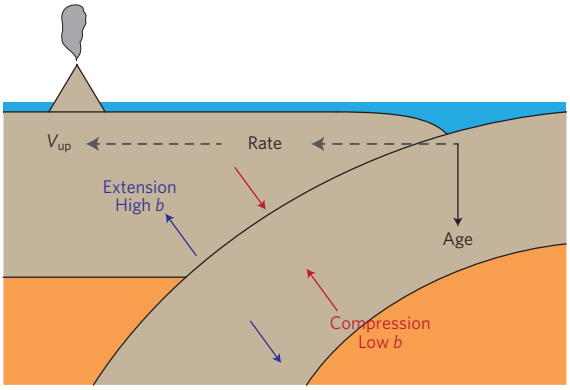

Figure 4 | Schematic diagram of a subduction zone. A young and buoyant slab produces high normal and shear stresses on the plate interface (red arrows), whereas an old and heavy slab produces lower stresses (blue arrows). The horizontal force balance, which the convergence rate or the upper plate velocity is thought to control, seems to have less influence on the stress state in subduction zones than the vertical balance, which is dominated by the slab buoyancy force. V_{up}; upper plate velocity with respect to the mantle.

lithosphere at about 80 Ma (refs 24,25). Oceanic lithosphere younger than about 80 Ma is cooling and thickening, whereas lithosphere older than about 80 Ma has thermally stabilized or experienced reheating events. Therefore, plate age and slab buoyancy are well correlated in slabs younger than about 80 Ma, but this correlation breaks down for older slabs. Consequently, the correlation between the *b*-value and plate age may become less clear for older slabs. In Supplementary Fig. 2, we compared the plate age and trench depth[25] (Supplementary Figs 1 and 3), which is thought to reflect the thickness of the lithosphere at the trench[26]. For details of the determination of the trench depth, see Methods. The goodness of the correlation between plate age and trench depth also seems to change between 60 Ma and 90 Ma ($R = 0.58$ for younger than 80 Ma and $R = 0.26$ for older than 80 Ma). Furthermore, Fig. 3d shows that the trench depth correlates well with the *b*-value. These results suggest that the change in the goodness of the correlation between plate age and *b*-value is due to the change in the growth rate of oceanic lithosphere and support the idea that *b*-values are mainly controlled by slab buoyancy.

An alternative explanation for the global variation in *b*-values may be the degree of complexity in subduction zone structure[15]. Low *b*-values in the eastern Pacific subduction zones are associated with a relatively simple coastline, and high *b*-values in the western Pacific island arcs are associated with complex island chains. However, our results show that the estimated *b*-values are particularly low in the subduction zones of the Solomon Islands and the New Hebrides in the western Pacific, where the subduction zone structures are complex and involve young subducting plates. Further quantitative investigations are necessary to evaluate the effects of complexity in subduction zone structures on *b*-values.

In some study regions in Sumatra and Tohoku, where M9-class earthquakes have occurred in recent years, the estimated *b*-values are lower than those expected from the overall trend of *b*-values for other subduction zones, which is determined by the subducting plate age (Fig. 3a). In Fig. 3d, *b*-values in Sumatra and Tohoku also seem to be lower than those in other subduction zones that have the same trench depths. This might reflect the high stress in the crust before the M9-class earthquakes[13]. In Sumatra, the *b*-value is particularly low near Siberut Island, where neither the 2004 Sumatra–Andaman earthquake nor the 2005 Nias–Simeulue earthquake ruptured[27]. Therefore, the source of this low *b*-value can be interpreted as either an ongoing stress accumulation near Siberut Island or past high stress in the crust before the 2004 Sumatra–Andaman earthquake.

Very large earthquakes and their aftershocks are often dominant in the seismic record, and the earthquake size distribution of aftershocks may be affected by changes in static stress caused by the mainshocks[28]. Therefore, we have also separately calculated *b*-values for triggered (aftershocks) and background events using the epidemic type aftershock sequence (ETAS) model[29,30] (Supplementary Fig. 4 and Table 1). Both *b*-values (that is, for triggered and background events) are comparable and correlate well with subducting plate age and trench depth and not with convergence rate and upper plate velocity, as is the case for *b*-values estimated using all events in each region (Supplementary Fig. 5). This suggests that the effect of stress change caused by mainshocks is negligible at the scale of our study. More details of the methods and discussion are described in Methods and Supplementary Information.

In addition to the primary control of slab buoyancy related to the plate age, *b*-values might also be dependent on temporal changes in stress and secondary tectonic factors, such as convergence rate, upper plate velocity, slab dip and geometrical irregularities along the plate interface. Although *b*-values do not directly predict the maximum earthquake size in each subduction zone, variations of the stress state in subduction zones worldwide, which cause variations of the *b*-value, may have some influences on the occurrence of great earthquakes; hence, understanding the physical properties and mechanisms that control spatial variations in the stress state and *b*-values may be useful for detecting stress accumulation due to an impending great earthquake. Assessments of earthquake hazards can be improved by monitoring the disparity between observed *b*-values and those expected from the physical properties of a subduction zone. Observed *b*-values that are much lower than those expected can be interpreted as indicating an additional stress accumulation in the crust, possibly related to an impending great earthquake.

Methods

Determination of M_c. We estimated M_c in each study region using the MAXC method and the MBS method, following ref. 20. We used the larger M_c to calculate *b*-values. In study regions where the difference between M_c values calculated using MAXC and MBS exceeds 0.5, we did not estimate *b*-values because of large uncertainties in M_c.

Determination of trench depth. We made about ten cross-sections in each trench section (Supplementary Fig. 3). The cross-sections extend ±50 km in the direction of the relative plate velocity from the trench. We defined the mean of the depth along all the cross-sections as the trench depth. We estimated the uncertainties from the deviation of the mean depth along each cross-section.

Sensitivity of the results to the choice of depth range and study regions. We repeated the analysis using only events shallower than 70 km to exclude the influence of anomalously deep events (Supplementary Fig. 6). To investigate the influence of the size and the selection of study regions, we also repeated the analysis using study regions cut in half (Supplementary Fig. 7). In both cases, the results were not strongly affected.

Consistency of results using the CMT catalogue and the ANSS catalogue. The ANSS catalogue is a composite catalogue, the heterogeneity of which may affect the estimation of *b*-values. Therefore, we also repeated the analysis using the CMT catalogue, which is more homogeneous than the ANSS catalogue, and checked the consistency of the results between the two catalogues (Supplementary Fig. 8 and Table 2). Because of the high M_c values for the CMT catalogue, there are insufficient events to calculate *b*-values precisely (for example, over 100 events) during 1978–2009 in most study regions in the CMT catalogue. Therefore, accepting large uncertainties, we calculated *b*-values in study regions with 20 and more events. The calculated *b*-values are positively correlated with plate age and trench depth, as is the case for the ANSS catalogue (Supplementary Fig. 8c,f). *b*-values for the CMT catalogue are systematically lower than *b*-values for the ANSS catalogue (Supplementary Fig. 8b). This might be due to the fact that it is not moment magnitude but rather body wave magnitude and surface wave magnitude that are used for many events in the ANSS catalogue. Body wave

magnitudes and surface wave magnitudes tend to saturate for larger events. On the other hand, moment magnitudes do not. This might lead to lower *b*-values in the CMT catalogue.

The estimation of the *b*-values for triggered events and background events. The earthquake size distribution of aftershocks may be different from that of background seismicity. Therefore, we calculated *b*-values for triggered and background events separately using the epidemic type aftershock sequence (ETAS) model[29]. The ETAS model expresses the seismicity rate ($\lambda(t)$) at time t as follows:

$$\lambda(t) = \mu + \sum_{t_i<t} \frac{Ke^{\alpha(M_i-M_c)}}{(t-t_i+c)^p}$$

where μ is the rate of the background seismicity and the second term is the contribution from preceding earthquakes of magnitude M_i ($M_i > M_c$) at time t_i ($t_i < t$) with four parameters (α, c, K and p). M_c is the minimum magnitude of the analysed catalogue. According to ref. 30, the probability of an event at time t being a background event is

$$P_b = \frac{\mu}{\lambda(t)}$$

Thus, the probability of an event at time t being a triggered event is

$$P_t = 1 - P_b$$

We estimated *b*-values for triggered events (b_t) and background events (b_b) by the weighted maximum-likelihood method using P_t and P_b as the weights. To estimate the uncertainty, we resampled events in each study region 1,000 times and calculated the mean of the variance of the *b*-values, which was estimated using the maximum-likelihood method[21].

Received 3 July 2014; accepted 1 October 2014; published online 2 November 2014

References

1. Molnar, P. & Atwater, T. Interarc spreading and Cordilleran tectonics as alternates related to the age of subducted oceanic lithosphere. *Earth Planet. Sci. Lett.* **41,** 330–340 (1978).
2. Ruff, L. & Kanamori, H. Seismicity and the subduction process. *Phys. Earth Planet. Inter.* **23,** 240–252 (1980).
3. Ruff, L. & Kanamori, H. Seismic coupling and uncoupling at subduction zones. *Tectonophysics* **99,** 99–117 (1983).
4. Scholz, C. H. & Campos, J. On the mechanism of seismic decoupling and back arc spreading at subduction zones. *J. Geophys. Res.* **100,** 22103–22115 (1995).
5. Gutenberg, B. & Richter, C. F. Frequency of earthquakes in California. *Bull. Seismol. Soc. Am.* **34,** 185–188 (1944).
6. Scholz, C. H. The frequency–magnitude relation of microfracturing in rock and its relation to earthquakes. *Bull. Seismol. Soc. Am.* **58,** 399–415 (1968).
7. Goebel, T. H. W. *et al.* Identifying fault heterogeneity through mapping spatial anomalies in acoustic emission statistics. *J. Geophys. Res.* **117,** B03310 (2012).
8. Goebel, T. H. W., Schorlemmer, D., Becker, T. W., Dresen, G. & Sammis, C. G. Acoustic emissions document stress changes over many seismic cycles in stick-slip experiments. *Geophys. Res. Lett.* **40,** 2049–2054 (2013).
9. Spada, M., Tormann, T., Wiemer, S. & Enescu, B. Generic dependence of the frequency-size distribution of earthquakes on depth and its relation to the strength profile of the crust. *Geophys. Res. Lett.* **40,** 709–714 (2013).
10. Schorlemmer, D., Wiemer, S. & Wyss, M. Variations in earthquake–size distribution across different stress regimes. *Nature* **437,** 539–542 (2005).
11. Wiemer, S. & Wyss, M. Mapping the frequency–magnitude distribution in asperities: An improved technique to calculate recurrence times? *J. Geophys. Res.* **102,** 15115–15128 (1997).
12. Ghosh, A., Newman, A. V., Thomas, A. M. & Farmer, G. T. Interface locking along the subduction megathrust from *b*-value mapping near Nicoya Peninsula, Costa Rica. *Geophys. Res. Lett.* **35,** L01301 (2008).
13. Nanjo, K. Z., Hirata, N., Obara, K. & Kasahara, K. Decade-scale decrease in *b* value prior to the *M*9-class 2011 Tohoku and 2004 Sumatra quakes. *Geophys. Res. Lett.* **39,** L20304 (2012).
14. Kagan, Y. Y. & Jackson, D. D. Tohoku earthquake: A surprise? *Bull. Seismol. Soc. Am.* **103,** 1181–1194 (2013).
15. Tsapanos, T. M. *b*-values of two tectonic parts in the circum-Pacific belt. *Pure Appl. Geophys.* **134,** 229–242 (1990).
16. Uyeda, S. & Kanamori, H. Back-arc opening and the mode of subduction. *J. Geophys. Res.* **84,** 1049–1061 (1979).
17. Heuret, A., Conrad, C. P., Funiciello, F., Lallemand, S. & Sandri, L. Relation between subduction megathrust earthquakes, trench sediment thickness and upper plate strain. *Geophys. Res. Lett.* **39,** L05304 (2012).
18. Ide, S. The proportionality between relative plate velocity and seismicity in subduction zones. *Nature Geosci.* **6,** 780–784 (2013).
19. Bird, P. An updated digital model of plate boundaries. *Geochem. Geophys. Geosyst.* **4,** 1027 (2003).
20. Woessner, J. & Wiemer, S. Assesing the quality of earthquake catalogues: Estimating the magnitude of completeness and its uncertainty. *Bull. Seismol. Soc. Am.* **95,** 684–698 (2005).
21. Aki, K. Maximum likelihood estimate of *b* in the formula $\log N = a - bM$ and its confidence limits. *Bull. Earthq. Res. Inst. Univ. Tokyo* **43,** 237–239 (1965).
22. Müller, R. D., Sdrolias, M., Gaina, C. & Roest, W. R. Age, spreading rates, and spreading asymmetry of the world's ocean crust. *Geochem. Geophys. Geosyst.* **9,** Q04006 (2008).
23. Argus, D. F., Gordon, R. G. & DeMets, C. Geologically current motion of 56 plates relative to the no-net-rotation reference frame. *Geochem. Geophys. Geosyst.* **12,** Q11001 (2011).
24. Parsons, B. & Sclater, J. G. An analysis of the variation of ocean floor bathymetry and heat flow with age. *J. Geophys. Res.* **82,** 803–827 (1977).
25. Smith, W. H. F. & Sandwell, D. T. Global sea floor topography from satellite altimetry and ship depth soundings. *Science* **277,** 1956–1962 (1997).
26. Hilde, T. W. C. & Uyeda, S. in *Geodynamics of the Western Pacific–Indonesian Region* (eds Hilde, T. W. C. & Uyeda, S.) 75–89 (AGU, 1983).
27. Scholz, C. H. & Campos, J. The seismic coupling of subduction zones revisited. *J. Geophys. Res.* **117,** B05310 (2012).
28. Gibowicz, S. J. Stress drop and aftershocks. *Bull. Seismol. Soc. Am.* **63,** 1433–1446 (1973).
29. Ogata, Y. Statistical models for earthquake occurrences and residual analysis for point processes. *J. Am. Stat. Assoc.* **83,** 9–27 (1988).
30. Zhuang, J., Ogata, Y. & Vere-Jones, D. Stochastic declustering of space–time earthquake occurrences. *J. Am. Stat. Assoc.* **97,** 369–380 (2002).

Acknowledgements

This work was supported by JSPS KAKENHI (23244090) and MEXT KAKENHI (21107007). Figures were prepared using Generic Mapping Tool (Wessel and Smith, 1998).

Author contributions

S.I. constructed a system for the statistical analysis of seismic sequences. T.N. analysed the data and wrote the paper.

Additional information

Supplementary information is available in the online version of the paper. Reprints and permissions information is available online at www.nature.com/reprints. Correspondence and requests for materials should be addressed to T.N.

Competing financial interests

The authors declare no competing financial interests.